Homeotic Arm-to-Leg Transformation Associated with Genomic Rearrangements at the *PITX1* Locus

Malte Spielmann,[1,2] Francesco Brancati,[3,4] Peter M. Krawitz,[1] Peter N. Robinson,[1] Daniel M. Ibrahim,[2,5] Martin Franke,[2] Jochen Hecht,[2,5] Silke Lohan,[1,2] Katarina Dathe,[1] Anna Maria Nardone,[4] Paola Ferrari,[6] Antonio Landi,[7] Lars Wittler,[8] Bernd Timmermann,[9] Danny Chan,[10] Ulrich Mennen,[11] Eva Klopocki,[1,2] and Stefan Mundlos[1,2,5,*]

The study of homeotic-transformation mutants in model organisms such as *Drosophila* revolutionized the field of developmental biology, but how these mutants relate to human developmental defects remains to be elucidated. Here, we show that Liebenberg syndrome, an autosomal-dominant upper-limb malformation, shows features of a homeotic limb transformation in which the arms have acquired morphological characteristics of a leg. Using high-resolution array comparative genomic hybridization and paired-end whole-genome sequencing, we identified two deletions and a translocation 5′ of *PITX1*. The structural changes are likely to remove active *PITX1* forelimb suppressor and/or insulator elements and thereby move active enhancer elements in the vicinity of the *PITX1* regulatory landscape. We generated transgenic mice in which *PITX1* was misexpressed under the control of a nearby enhancer and were able to recapitulate the Liebenberg phenotype.

Introduction

During development, the forelimb and hindlimb buds of tetrapods are morphologically uniform. However, as limb development proceeds, each individual tissue attains a characteristic morphology that ultimately defines the identity of a forelimb (arm) or a hindlimb (leg).[1,2] In humans, for example, the elbow has two functions: in one plane, it acts as a hinge stabilized via the olecranon, and it also rotates (pronates or supinates) the forearm. The knee, in contrast, functions as a mobile hinge joint permitting flexion and extension, as well as a slight medial and lateral rotation stabilized by an additional flexible bone, the patella. Similar characteristic features distinguish the small wrist (carpal) bones from the large foot (tarsal) bones. Forelimb versus hindlimb identity and the development of their specific morphology are governed by a specific set of regulatory genes, mainly of the Hox and T-box families.[1,3]

Liebenberg syndrome (MIM 186550) is characterized by the combination of dysplastic elbow joints and the fusion of wrist bones and the consequent radial deviation.[4] Here, we show that in this human limb-malformation syndrome, the upper extremities have undergone a partial homeotic transformation and have acquired features of the lower limbs.

Subjects and Methods

Human Subjects

All individuals were enrolled in the study under an informed-consent protocol approved by the institutional review board at Jacaranda Hospital in Muckleneuk, the Policlinico Tor Vergata University Hospital in Rome, or the Policlinico of Modena.

Genome-wide SNP Genotyping

We genotyped DNA samples from ten individuals of family 1 by using the Affymetrix GeneChip Human Mapping 10K Array, v.2.0 (Affymetrix, Santa Clara, CA) and performed a genome-wide linkage analysis as described previously.[5] Genotypes were called by GeneChip DNA Analysis Software v.2.0 (Affymetrix). Relationship errors were evaluated with the help of the program Graphical Relationship Representation. The program PedCheck was applied for detecting Mendelian errors, and the data for SNPs with such errors were removed from the data set. Non-Mendelian errors were identified with the program MERLIN, and unlikely genotypes for related samples were deleted. Parametric linkage analysis was performed with a modified version of the program GENEHUNTER 2.1. Assuming autosomal-dominant inheritance with full penetrance and a disease allele frequency of 0.0001, we used a sliding window with sets of 90 SNPs for calculation. All data handling was performed with the graphical user interface ALOHOMORA. Microsatellite markers were used for confirming the interval.

[1]Institute for Medical Genetics and Human Genetics, Charité–Universitätsmedizin Berlin, 13353 Berlin, Germany; [2]Research Group of Development & Disease, Max Planck Institute for Molecular Genetics, 14195 Berlin, Germany; [3]Istituto di Ricovero e Cura a Carattere Scientifico, Casa Sollievo della Sofferenza Hospital, Casa Sollievo della Sofferenza Hospital-Mendel Institute, 00198 Rome, Italy; [4]Policlinico Tor Vergata University Hospital, 00198 Rome, Italy; [5]Berlin-Brandenburg Center for Regenerative Therapies, 13353 Berlin, Germany; [6]Department of Pediatrics, University of Modena and Reggio Emilia, 41100 Modena, Italy; [7]Hand Surgery and Microsurgery Unit, Policlinico of Modena, 41100 Modena, Italy; [8]Developmental Genetics, Max Planck Institute for Molecular Genetics, 13353 Berlin, Germany; [9]Next-Generation Sequencing Group, Max Planck Institute for Molecular Genetics, 14195 Berlin, Germany; [10]Department of Biochemistry, The University of Hong Kong, Pokfulam, Hong Kong; [11]Jacaranda Hospital, Muckleneuk, Pretoria 0083, South Africa
*Correspondence: stefan.mundlos@charite.de
http://dx.doi.org/10.1016/j.ajhg.2012.08.014.

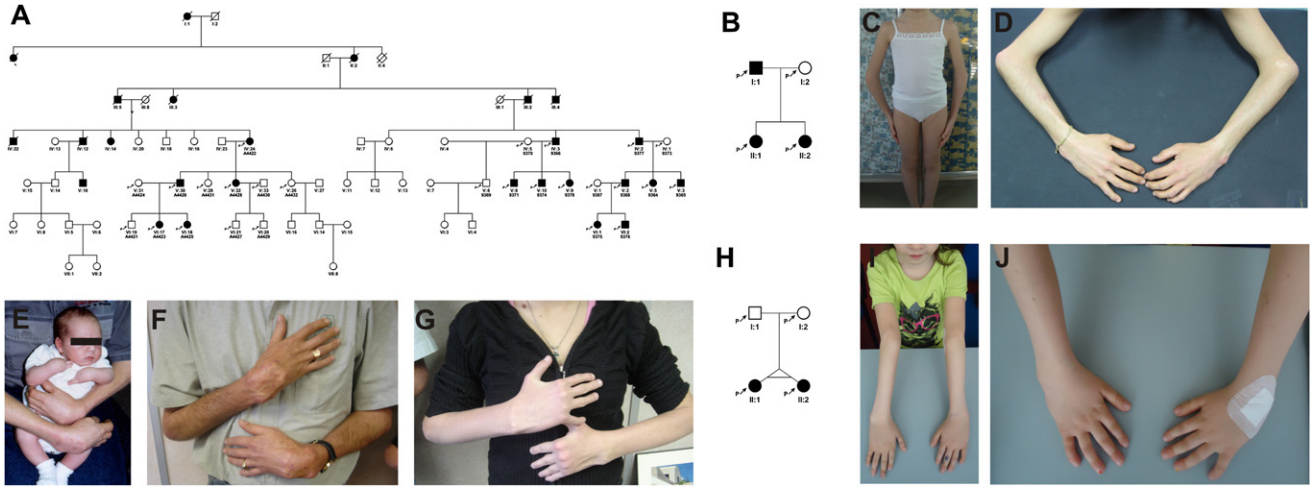

Figure 1. Pedigrees and Clinical Phenotypes of Three Unrelated Families Affected by Liebenberg Syndrome
(A, B, and H) Pedigrees of Liebenberg-syndrome-affected families: family 1 (A), family 2 (B), and family 3 (H). Affected individuals are indicated by black symbols. Symbols with a "p" indicate individuals who were clinically examined and for whom further molecular analysis was performed.
(C–G and J) Clinical presentation of affected individuals. Note radial deviation of hands and enlargement of wrists (E–G, I, and J). The elbows show flexion deformity causing the inability to fully straighten the joint and an appearance resembling anterior dislocation (C and D).

Next-Generation Sequencing and Data Processing for Breakpoint Detection

The whole genome of patient II:1 from family 3 was sequenced by a 100 bp paired-end run on Illumina's HiSeq 2000 platform and yielded 40 Gb of raw sequence data. The sequence reads were mapped to the human reference GRCh37.3 with Novoalign in paired-read mode.[6] The alignment was filtered for translocated reads defined as paired reads that mapped to different chromosomes. The majority of these 949,840 translocated reads represent artifacts that originate from in vitro fragment ligation. The distribution of these reads over the genome is well described by a Poisson distribution. In order to identify potential breakpoints of translocated chromosomes, we filtered for a significant enrichment of such translocated reads in a window size of 500 bp, representing half of the mean fragment size. The region with the highest significance (14 translocated reads) indicated a breakpoint between chr5: 134,587,342–134,587,490 and chr18: 43,049,294–43,049,395 (Figure S2, available online).

The exact breakpoints were confirmed by Applied Biosystems Sanger sequencing. In order to detect the exact breakpoint from the next-generation sequencing (NGS) whole-genome data set, we then mapped all reads that did not align to the reference sequence hg19 to templates with potential breakpoints. Figure S3 shows an Integrated Genomics Viewer screenshot of two reads that map to a template on the derivative chromosome 5 at hg19 (chr5: 134,587,334; chr18: 43,049,644) and 11 reads that map to a template on the derivative chromosome 18 at hg19 (chr18: 43,049,293; chr5: 134,587,638). All primers are available on request.

Array CGH

Microarray-based comparative genomic hybridization (array CGH) was carried out with a custom-designed array (Agilent Technologies, Santa Clara, CA) that covers the linkage region from 122 to 136 Mb on human chromosome 5 at a high density, as previously described.[7]

Generation of Single-Copy *hs1473-PITX1* Transgenic Mice

We generated single-copy transgenic mice by using the C2 embryonic stem cell (ESC) line developed by Thermo Scientific Open Biosystems (Thermo Scientific Open Biosystems Gene Targeting Kit).[8,9] To facilitate targeting to the flippase recognition target (FRT)-flanked ColA1 locus, we used the PGK-ATG-FRT vector to clone the hs1473 enhancer region upstream of a *PITX1* minigene driven by an *Hsp68* minimal promoter. In the presence of flippase recombinase, this vector has been designed to be inserted at the FRT site along with a PGK promoter and an ATG initiation codon upstream and in frame with the hygromycin resistance gene, and it thereby confers hygromycin resistance to the correctly targeted cell. Positive ESC clones were screened with Southern blot analysis. Mice were generated by tetraploid ESC aggregation. At embryonic day (E) 15.5, the mice were sacrificed and skeletal preparations of the embryos were performed. All animal procedures were in accordance with institutional, state, and government regulations (Berlin: LAGeSo).

Results

Arm-to-Leg Transformation in Liebenberg Syndrome

We investigated three unrelated families affected by Liebenberg syndrome (Figures 1A–1H). After initial inspection of the phenotype, we performed in-depth imaging of the skeletal and soft-tissue abnormalities. In the normal elbow, the distal head of the humerus articulates with the ulna at the trochlear notch, and the olecranon process of the ulna extends proximally from the elbow joint (Figure 2A). In the affected subjects, the olecranon was hypoplastic or missing (Figures 2B–2D), and the distal humerus and the proximal head of the ulna were broadened (Figures 2B and 2C) such that the distal humerus

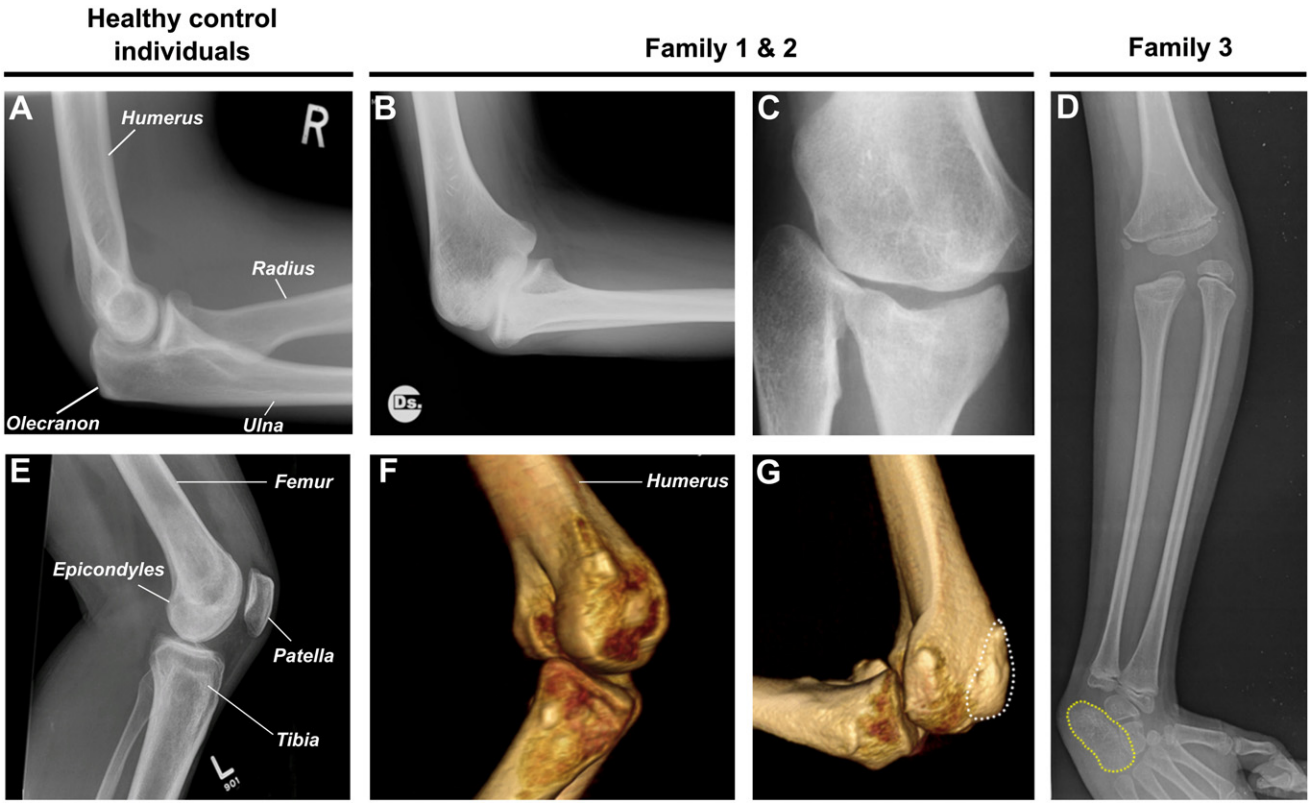

Figure 2. The Liebenberg Phenotype Is Characterized by a Partial Homeotic Arm-to-Leg Transformation
Lateral X-ray of a normal elbow (A) and knee (E). Note the anatomical differences between the elbow (olecranon) and knee (patella) joints. In families 1 and 2, the olecranon is hypoplastic and the distal humerus is broadened at the elbow (B) and resembles the shape of a femur (E). The proximal head of the ulna is broadened (C) similarly to the tibial plateau of the knee joint. Three-dimensional computed tomography (CT) scans show a patella-like structure fused to the distal head of the humerus (G, outlined in white). The distal humerus has a medial and lateral condyle (F) separated by an intercondylar fossa (trench) resembling the femoral epicondyles of the knee. In family 3, the arm-to-leg-transformation phenotype is even more severe. The olecranon is completely missing (D), and the fusion of the triquetral and pisiform (D, outlined in yellow) forms an element that is similar not only in shape but also in size to the calcaneus in the ankle.

resembled the distal head of the femur and the proximal ulna resembled the proximal head of the tibia. (Figures 2B, 2C, and 2E). Three-dimensional computed tomography (CT) scans of the humerus showed a medial and lateral condyle separated by an intercondylar fossa (Figure 2F) resembling the femoral epicondyles of the knee (Figure 2E) and a patella-like structure fused to the distal head of the humerus (Figure 2G, outlined in white). The joint surface of the radius and ulna was flat and resembled that of the tibia and fibula. In family 3, the arm-to-leg-transformation phenotype is even more severe. In family 3, the fusion of the triquetral and pisiform (Figure 2D, outlined in yellow) formed an element that is similar in shape and size to the calcaneus of the ankle.

In addition, the bones of the hand and wrist were highly abnormal. Radiographs of the hands showed long metacarpals resembling the metatarsals of the feet (Figure 3A). Fusion of the triquetral and pisiform (outlined in yellow in Figures 3A and 3D and red arrow in Figure 3E) led to a structure similar in shape to the calcaneus of the ankle. In addition, the scaphoid and lunate bones were fused (Figure 3D, outlined in red) and formed an element that was similar to the shape of the talus in the ankle. The arm-to-leg transformation additionally encompasses specific muscles and tendons. The extensor minimi digiti muscle straightens the little finger and is only present in the hand, but not in the foot. This muscle and its tendon were absent in the hands of Liebenberg individuals (Figure 3 B, indicated by yellow line). Similarly, the extensor carpi radialis muscle, a characteristic muscle of the hand, and its two tendons were absent in the Liebenberg individuals (indicated by a red line in Figure 3B).

Liebenberg Syndrome Is Associated with Structural Variations at the *PITX1* Locus

Genome-wide SNP genotyping (Affymetrix, Santa Clara, CA) in family 1 revealed a candidate region of 9.8 Mb in chromosomal region 5q23-31 between markers rs1366100 and rs2107331. Exome enrichment of region 5q23-31 followed by high-throughput sequencing did not identify a disease-causing mutation. Custom high-resolution array CGH analysis, however, revealed a heterozygous 134 kb deletion (chr5: 134,624,602–134,759,492; hg19; DECIPHER BER266643) (Figure 4A and Figure S1).

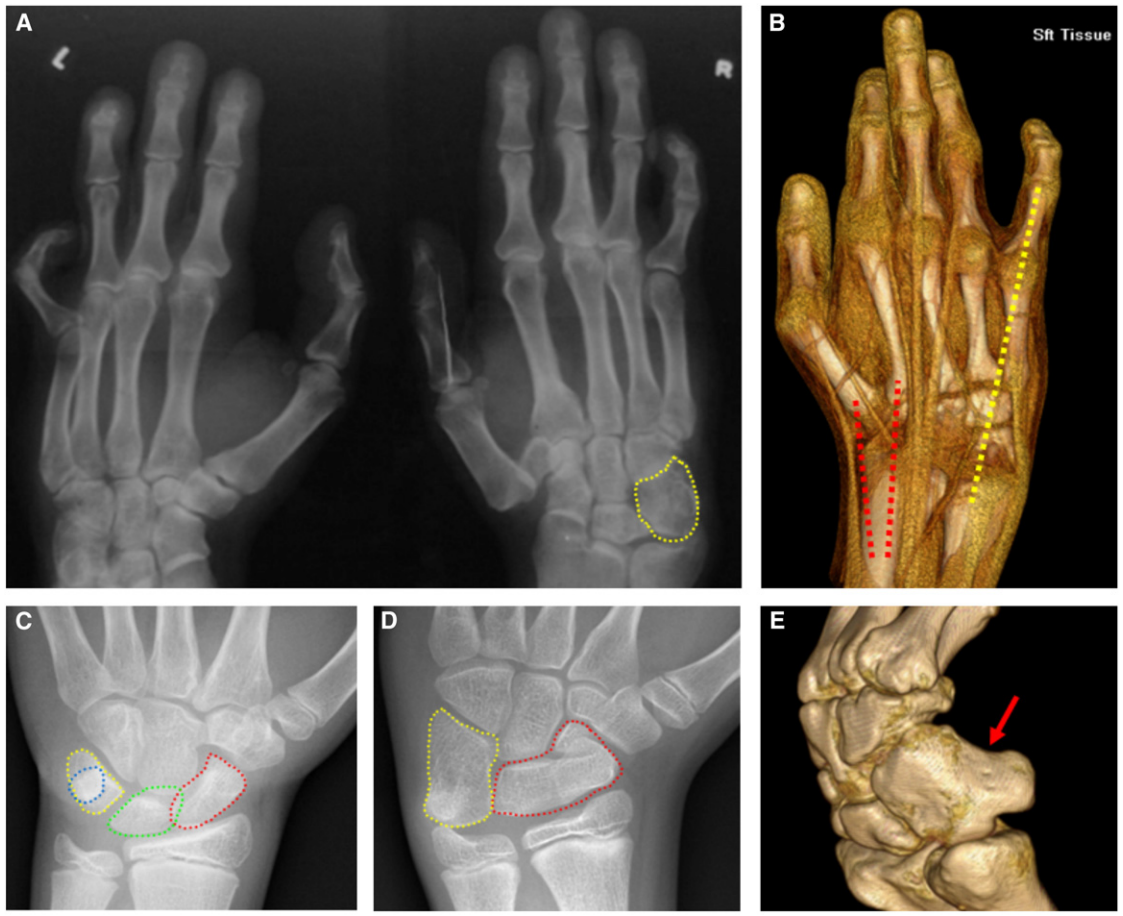

Figure 3. The Bones and Muscles of the Wrist Are Abnormal and Have Acquired Features Characteristic of the Ankle
X-rays of the hands show elongated metacarpals resembling the metatarsals of the feet (A). In families 1 and 2, the apparent fusion of the triquetral and pisiform (A and D [outlined in yellow] and E [red arrow]) forms a structure similar in shape to the calcaneus of the ankle. These are separate bones in the normal wrist (C, yellow and blue). In addition, the scaphoid and lunate bones are fused (outlined in red in D and in red and green, respectively, in C) and form an element that is similar to the shape of the talus in the ankle. The arm-to-leg transformation additionally encompasses specific muscles and tendons. The extensor minimi digiti muscle straightens the little finger and is only present in the hand, but not in the foot. This muscle and its tendon are absent in the hands of Liebenberg individuals (B, indicated by yellow line). Similarly, the extensor carpi radialis muscle, a characteristic muscle of the hand, and its two tendons are absent in the Liebenberg individuals (B, indicated by red lines).

The deleted region encompasses *H2AFY* (MIM 610054) and is located 269 kb 5′ of *PITX1* (MIM 602149). Array CGH analysis of unrelated family 2 showed an overlapping heterozygous 107 kb deletion (chr5: 134,638,524–134,746,407; hg19; DECIPHER BER266644) (Figure 4A and Figure S1). However, we were not able to identify any relevant copy-number variation in family 3. In order to detect translocations or inversions, we performed paired-end whole-genome sequencing. Whole-genome NGS indicated a translocation between chromosomes 5 and 18. The predicted translocation—t(5;18)(q31.1; q12.3)—was confirmed by Sanger sequencing and fluorescent in situ hybridization (Figure S4).

The translocation was associated with a 303 bp deletion on chromosome 5 (chr5: 134,587,335–134,587,637) and a 350 bp deletion on chromosome 18 (chr18: 43,049,294–43,049,643). Neither sequence included any coding sequence or any highly conserved noncoding elements. The breakpoint on the derivative chromosome 5 is located in the gene desert neighboring *PITX1* (Figure 4B and Figure S2) at hg19 (chr5:134,587,334; chr18: 43,049,644) and on derivative chromosome 18 at hg19 (chr18: 43,049,293; chr5: 134,587,638). The deletions in families 1 and 2 encompass the entire ubiquitously expressed *H2AFY*, which encodes for macroH2A1. In family 3, the translocation moves *H2AFY* to chromosome 18. The deletion of *H2AFY* is unlikely to be causative because the homozygous inactivation of *H2afy* in mice leads to hepatic accumulation of lipids but does not result in a bone or limb phenotype.[11]

Alterations of the Regulatory Landscape at the PITX1 Locus

A screen of the *cis*-regulatory landscape surrounding the deletion and the translocation with the use of the Vista Enhancer Database revealed one highly conserved

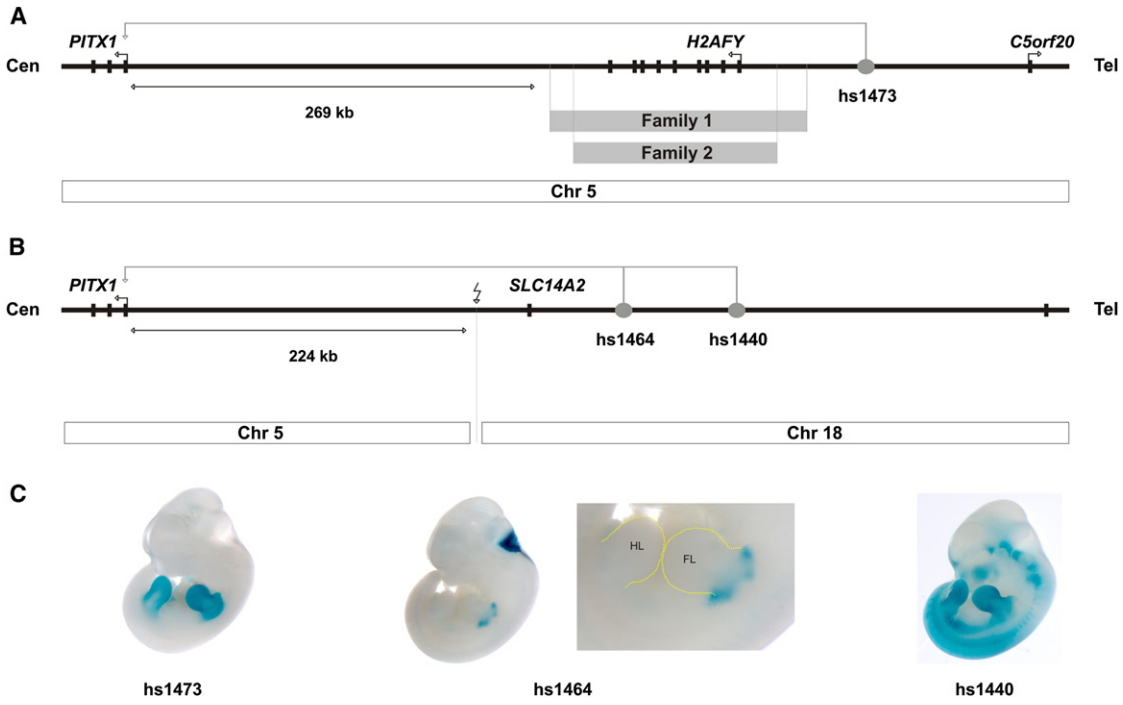

Figure 4. Genomic Rearrangements Appear to Result in a Misexpression of *PITX1* in the Forelimb via the Activation of Ectopic Enhancers

(A) Array CGH analysis in families 1 and 2 revealed overlapping heterozygous chromosome 5 deletions located 5′ of *PITX1* and separated only by a gene desert. The Vista Enhancer Database indicates one highly conserved noncoding element hs1473 10 kb telomeric of the deleted region that shows forelimb- and hindlimb-specific enhancer activity (C) in E11.5 transgenic mouse embryos.[10]

(B) In family 3, paired-end whole-genome sequencing revealed a translocation, t(5;18)(q31.1;q12.3). Enhancer element hs1464, telomeric of the breakpoint, shows proximal forelimb-specific enhancer activity (C), and hs1440 shows forelimb- and hindlimb–specific enhancer activity[7] (C).

noncoding element 10 kb telomeric of the deleted region. We show that this enhancer element hs1473 shows limb-specific (forelimb and hindlimb) activity in E11.5 transgenic mouse embryos[10] (Figure 4C). Furthermore, the Vista Enhancer Database revealed that in family 3 two highly conserved noncoding elements, i.e., hs1464 and hs1440, from chromosome 18 were translocated upstream of *PITX1* on derivative chromosome 5 (Figure 4B). The human enhancer element hs1464 located 83 kb telomeric of the breakpoint shows proximal forelimb-specific enhancer activity (Figure 4C), and the element hs1440 located 118 kb telomeric of the breakpoint shows forelimb- and hindlimb-specific activity (Figure 4C).[7] Thus, the structural rearrangements result in the relocation of limb-specific enhancer element(s) into the gene desert that is 5′ of *PITX1* and that potentially affects PITX1 expression.

In order to test whether enhancer hs1473 is able to produce a Liebenberg-like phenotype, we generated single-copy transgenic mice. At E15.5, *hs1473-Pitx1* transgenic embryos showed characteristic features of Pitx1 misexpression resulting in a forelimb-to-hindlimb transformation (Figure 5). The mice showed loss of the olecranon (Figure 5, black arrow) and thus recapitulated the Liebenberg phenotype. Only one zeugopod bone was present. The distal head of the humerus was more similar to the distal femur, and the shape of the proximal head of the single zeugopodal element resembled the shape of the proximal tibia (Figure 5, red arrow). Two digits were missing, and the remaining digit I had two phalanges and was fused to the metacarpal of digit II. Fusions of the carpals formed a structure similar in shape to the calcaneus of the hindlimb (Figure 5, green arrows). The fusion of the carpals and radial deviation of the hands caused a foot-like appearance of the forelimb.

Discussion

We show that Liebenberg syndrome is characterized by a partial homeotic transformation of the upper extremities, a phenotype which is associated with genomic rearrangements at the *PITX1* locus. Similar phenotypes have previously been observed in animal models. Logan et al. described a forelimb-to-hindlimb transformation in chick wing buds in which PITX1 was misexpressed.[12] Furthermore, misexpression of Pitx1 in the forelimb of mice with the use of the *Prx1* promoter results in a phenotype identical to that observed in our mice.[13] Similar to the Liebenberg phenotype, the transformation also included specific muscles, such as the extensor carpi radialis muscle, giving the forelimbs a hindlimb-like morphology.

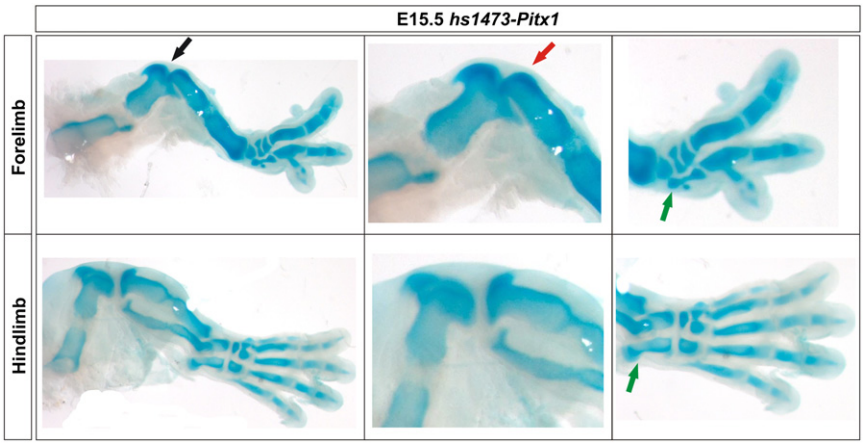

Figure 5. E15.5 *hs1473-Pitx1* Transgenic Embryos Showed Characteristic Features of a Forelimb-to-Hindlimb Transformation

The mice showed loss of the olecranon (black arrow) and thus recapitulated the Liebenberg phenotype. Only one zeugopod bone was present. The distal head of the humerus was more similar to the distal femur, and the shape of the proximal head of the single zeugopodal element resembles the shape of the proximal tibia (red arrow). Two digits were missing, and the remaining digit I had two phalanges and was fused to the metacarpal of digit II. Fusions of the carpals formed a structure similar in shape to the calcaneus of the hindlimb (Figure 4, green arrows). Fusion of the carpals and radial deviation of the hands caused a foot-like appearance of the forelimb.

However, the loss of one zeugopodal element and the loss of two digits were Pitx1-dose dependent and were observed only in homozygous mice. Therefore, it is likely that enhancer hs1473 used in our study shows a strong limb-specific activity resulting in relatively high levels of Pitx1. *Cis*-acting regulatory changes at the *PITX1* locus have also been described in the evolution of sticklebacks, and the deletion of enhancer element *Pel* has been shown to cause a loss of *PITX1* expression in the pelvic region.[14]

We hypothesize that the arm-to-leg transformation observed in affected subjects from families segregating Liebenberg syndrome is due to misexpression of PITX1 in the upper extremities. The structural changes are likely to remove active *PITX1* forelimb suppressor and/or insulator elements and thereby move active enhancer elements in the vicinity of the *PITX1* regulatory landscape. Although we could not directly observe this postulated misexpression in our study subjects because it probably occurred during their early development, we could recapitulate the identical phenotype in mice by such misexpression (Figure 5). The difference we observed in the phenotypic severity between families 1 and 2 compared to family 3 might be due to the different tissue specificities of enhancer element hs1473 versus hs1464 and hs1440. Whereas hs1473 might regulate the nearby *H2AFY*, elements hs1464 and hs1440 on chromosome 18 are probably regulators of *SETBP1* (MIM 611060), which is expressed in developing forelimbs and hindlimbs.[15,16]

The transformation of one body part into another is also called homeosis and has been described for *Drosophila* mutants resulting from mutations in or misexpression of Hox genes.[17,18] Homeotic transformations of the vertebrae have also been observed in mice in association with the inactivation of certain paralogous Hox genes.[19,20] Liebenberg syndrome is a human condition with a true homeotic limb transformation affecting the morphology of the entire extremity, including bones and joints, as well as muscles and tendons. As shown here, structural variations can result in the reprogramming of basic developmental processes. Genomic rearrangements linked to *PITX1* might also contribute to evolutionary changes of limb structures in humans and other tetrapods.

Supplemental Data

Supplemental Data include four figures and can be found with this article online at http://www.cell.com/AJHG.

Acknowledgments

We would like to thank the families for their collaboration and contribution to this project. We acknowledge F. Trotier, R. Koll, and B. Teubner for technical assistance. We thank A. Proietti for her assistance with our patients. This project was supported by a grant from the Deutsche Forschungsgemeinschaft to S.M. and E.K.

Received: June 19, 2012
Revised: July 31, 2012
Accepted: August 14, 2012
Published online: September 27, 2012

References

1. Ouimette, J.F., Jolin, M.L., L'honoré, A., Gifuni, A., and Drouin, J. (2010). Divergent transcriptional activities determine limb identity. Nat. Commun. *1*, 35.
2. Duboc, V., and Logan, M.P. (2011). Regulation of limb bud initiation and limb-type morphology. Dev. Dyn. *240*, 1017–1027.
3. Logan, M. (2003). Finger or toe: The molecular basis of limb identity. Development *130*, 6401–6410.
4. Liebenberg, F. (1973). A pedigree with unusual anomalies of the elbows, wrists and hands in five generations. S. Afr. Med. J. *47*, 745–748.
5. Dathe, K., Kjaer, K.W., Brehm, A., Meinecke, P., Nürnberg, P., Neto, J.C., Brunoni, D., Tommerup, N., Ott, C.E., Klopocki, E., et al. (2009). Duplications involving a conserved regulatory element downstream of BMP2 are associated with brachydactyly type A2. Am. J. Hum. Genet. *84*, 483–492.

6. Etter, P.D., Preston, J.L., Bassham, S., Cresko, W.A., and Johnson, E.A. (2011). Local de novo assembly of RAD paired-end contigs using short sequencing reads. PLoS ONE *6*, e18561.
7. Visel, A., Minovitsky, S., Dubchak, I., and Pennacchio, L.A. (2007). VISTA Enhancer Browser—a database of tissue-specific human enhancers. Nucleic Acids Res. *35* (Database issue), D88–D92.
8. Beard, C., Hochedlinger, K., Plath, K., Wutz, A., and Jaenisch, R. (2006). Efficient method to generate single-copy transgenic mice by site-specific integration in embryonic stem cells. Genesis *44*, 23–28.
9. Artus, J., and Hadjantonakis, A.K. (2011). Generation of chimeras by aggregation of embryonic stem cells with diploid or tetraploid mouse embryos. Methods Mol. Biol. *693*, 37–56.
10. Pennacchio, L.A., Ahituv, N., Moses, A.M., Prabhakar, S., Nobrega, M.A., Shoukry, M., Minovitsky, S., Dubchak, I., Holt, A., Lewis, K.D., et al. (2006). In vivo enhancer analysis of human conserved non-coding sequences. Nature *444*, 499–502.
11. Boulard, M., Storck, S., Cong, R., Pinto, R., Delage, H., and Bouvet, P. (2010). Histone variant macroH2A1 deletion in mice causes female-specific steatosis. Epigenetics Chromatin *3*, 8.
12. Logan, M., and Tabin, C.J. (1999). Role of Pitx1 upstream of Tbx4 in specification of hindlimb identity. Science *283*, 1736–1739.
13. DeLaurier, A., Schweitzer, R., and Logan, M. (2006). Pitx1 determines the morphology of muscle, tendon, and bones of the hindlimb. Dev. Biol. *299*, 22–34.
14. Chan, Y.F., Marks, M.E., Jones, F.C., Villarreal, G., Jr., Shapiro, M.D., Brady, S.D., Southwick, A.M., Absher, D.M., Grimwood, J., Schmutz, J., et al. (2010). Adaptive evolution of pelvic reduction in sticklebacks by recurrent deletion of a Pitx1 enhancer. Science *327*, 302–305.
15. Suphapeetiporn, K., Srichomthong, C., and Shotelersuk, V. (2011). SETBP1 mutations in two Thai patients with Schinzel-Giedion syndrome. Clin. Genet. *79*, 391–393.
16. Hoischen, A., van Bon, B.W., Gilissen, C., Arts, P., van Lier, B., Steehouwer, M., de Vries, P., de Reuver, R., Wieskamp, N., Mortier, G., et al. (2010). De novo mutations of SETBP1 cause Schinzel-Giedion syndrome. Nat. Genet. *42*, 483–485.
17. Shimell, M.J., Simon, J., Bender, W., and O'Connor, M.B. (1994). Enhancer point mutation results in a homeotic transformation in Drosophila. Science *264*, 968–971.
18. Emerald, B.S., and Roy, J.K. (1997). Homeotic transformation in Drosophila. Nature *389*, 684.
19. Wellik, D.M., and Capecchi, M.R. (2003). Hox10 and Hox11 genes are required to globally pattern the mammalian skeleton. Science *301*, 363–367.
20. Horan, G.S., Wu, K., Wolgemuth, D.J., and Behringer, R.R. (1994). Homeotic transformation of cervical vertebrae in Hoxa-4 mutant mice. Proc. Natl. Acad. Sci. USA *91*, 12644–12648.